The observed influence of local anthropogenic pollution on northern Alaskan cloud properties

Maximilian Maahn[1,2], Gijs de Boer[1,2], Jessie M. Creamean[1,2], Graham Feingold[2], Greg M. McFarquhar[3], Wei Wu[3,4], and Fan Mei[5]

[1]University of Colorado, Cooperative Institute for Research in Environmental Sciences, Boulder, Colorado, USA
[2]National Oceanographic and Atmospheric Administration, Earth System Research Laboratory, Boulder, Colorado, USA
[3]University of Illinois at Urbana-Champaign, Urbana, Illinois, USA
[4]National Center for Atmospheric Research, Boulder, Colorado, USA
[5]Pacific Northwest National Laboratory, Richland, Washington, USA

Correspondence to: Maximilian Maahn (maximilian.maahn@colorado.edu)

Abstract.

Due to their importance for the radiation budget, liquid-containing clouds are a key component of the Arctic climate system. Depending on season, they can cool or warm the near-surface air. The radiative properties of these clouds depend strongly on cloud drop sizes, which are governed by the availability of cloud condensation nuclei. Here, we investigate how cloud drop sizes are modified in the presence of local emissions from industrial facilities at the North Slope of Alaska. For this, we use aircraft in-situ observations of clouds and aerosols from the 5th Department of Energy Atmospheric Radiation Measurement (DOE ARM) Program's Airborne Carbon Measurements (ACME-V) campaign obtained in Summer 2015. Comparison of observations from an area with petroleum extraction facilities (Oliktok Point) with data from a reference area relatively free of anthropogenic sources (Utqiaġvik/Barrow) represents an opportunity to quantify the impact of local industrial emissions on cloud properties. In the presence of local industrial emissions, the mean effective radii of cloud droplets are reduced from 12.2 to 9.8 μm, which leads to a suppression of drizzle production and precipitation. At the same time, concentrations of refractory black carbon and condensation nuclei are enhanced below the clouds. These results demonstrate that the effects of anthropogenic pollution on local climate need to be considered when planning Arctic industrial infrastructure in a warming environment.

1 Introduction

Liquid-containing clouds are a significant modulator of the Arctic climate system's radiation budget. Their properties impact both shortwave and longwave radiative transfer, resulting in seasonally-dependent influences that include both net cooling and warming of the Arctic surface (Intrieri et al., 2002; Shupe and Intrieri, 2004), and various forms of cloud feedbacks (Colman, 2003). At the same time, liquid cloud droplet number concentration and size are influenced by the number of available cloud condensation nuclei. It has been proposed that this has an effect on cloud albedo, life cycle and longwave emissivity (Twomey, 1976; Albrecht, 1989; Garrett and Zhao, 2006). Long range transport of aerosol particles from lower latitudes in winter and

early spring (Arctic haze) and episodic forest fires in summer can lead to higher aerosol concentrations (Shaw, 1995; Law and Stohl, 2007), which have been found to modify liquid and mixed phase cloud properties (Garrett et al., 2004; McFarquhar et al., 2011; Jackson et al., 2012; Zamora et al., 2016). Besides these transported emissions, the Arctic is an environment that is generally relatively clean (Quinn et al., 2002, 2009) which makes clouds particularly susceptible to an increase in aerosol concentration (Platnick and Twomey, 1994). In comparison to other regions, there are only few sources of local anthropogenic emissions north of the Arctic Circle, which are mainly related to ship traffic and petroleum as well as natural gas extraction facilities (Law and Stohl, 2007). While emissions from ships are expected to rise due to the retreating sea ice, emissions from resource extraction are expected to remain at present day levels (Peters et al., 2011) with an estimated 13% of the world's untapped oil resources located in the Arctic (Gautier et al., 2009). Local emissions by Arctic petroleum and natural gas extraction facilities have been observed and quantified by aircraft campaigns (Brock et al., 2011; Roiger et al., 2015). These emissions are mostly associated with flaring, but also by regular internal combustion engines. Ødemark et al. (2012) found that black carbon (BC), which is particularly created by flaring (Stohl et al., 2013), results in a modeled positive net radiative forcing of petroleum and natural gas extraction, mainly due to deposition of BC on the snow. Kolesar et al. (2017) showed that emissions from the Prudhoe Bay area result in in-situ particle growth events in Barrow, located around 300 km west of the Prudhoe Bay region. Although these previous studies have demonstrated the potential impact from industrial activities in the Arctic, in-situ aerosol and cloud observations have not been combined in order to study local sources of emissions.

In this work, we show how cloud properties are altered by aerosol particles originating from local anthropogenic pollution from industrial activities in the Prudhoe Bay area in northern Alaska (Fig. 1), and investigate the influence on processes impacting the cloud life cycle. Even though the work is limited to observations from the North Slope of Alaska, the results are broadly applicable to other Arctic regions with significant industrial activities (e.g. Siberia), although exact details of the types of aerosol effects will be influenced by aerosol concentration, size, and composition. Because of their importance in regulating the surface and top-of-atmosphere energy budgets, we focus here on liquid clouds. Increased cloud droplet concentrations in the Prudhoe Bay, Alaska area were previously reported by Hobbs and Rangno (1998) although that study could not directly connect these increased concentrations to locally produced aerosol particles due to a lack of aerosol measurements. In this study, we fill this gap by using airborne cloud property and aerosol observations obtained during the US Department of Energy Atmospheric Radiation Measurement (DOE ARM) program's 5th ARM Airborne Carbon Measurements (ACME-V) campaign to study the influence of local pollution on Arctic liquid clouds. An enhanced understanding of the influence is crucial to evaluate the role of clouds and aerosols in changing Arctic which is warming faster than other regions (Jeffries et al., 2013)

In Section 2 we provide background information on the ACME-V campaigns along with details on the various data sets used to conduct our analysis. Following this, we analyze observed aerosol particle (Section 3) and cloud (Section 4) properties, before combining these to evaluate the interactions between locally-produced aerosols and clouds in Section 5. This evaluation is carried further in Section 6 where we attempt to quantify observed aerosol-cloud interactions. Finally, we provide a summary and concluding remarks in Section 7.

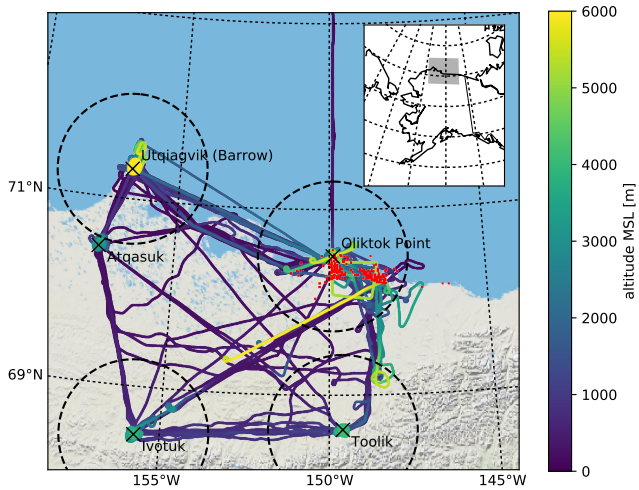

Figure 1. Overview of all flights of the ACME-V campaign. Color shows altitude m MSL. The dashed circles indicate 90 km radii around the sites (black crosses), the red dots indicate active oil wells (Data obtained from http://doa.alaska.gov/ogc/publicdb.html in March 2017)

2 Data set

The ACME-V aircraft campaign took place from June to September 2015 (Biraud et al., 2016) and consisted of 38 research flights of the ARM Gulfstream G-159 (G-1) aircraft of the ARM aerial facility (Schmid et al., 2014, 2016). Since the campaign targeted trace gas measurements from local and regional sources, a majority of the flight time was spent below 200 m above mean sea level (MSL). However, spirals up to an altitude of 6,000 m were flown in the vicinity of two ARM surface observatories in northern Alaska, Utqiaġvik (formerly known as Barrow or North Slope of Alaska, NSA, 71.323°N, 156.616°W) and Oliktok Point (OLI, 70.495°N, 149.886°W). Additional spirals were flown at Toolik (68.628°N, 149.598°W), Ivotuk (68.483°N, 155.754°W), and Atqasuk (70.467°N, 157.436°W) in order to characterize cloud and aerosol properties (Fig.1). In this work, we compare data within 90 km of OLI and NSA. These two sites form an ideal opportunity to study the effects of local emissions on cloud properties: While OLI is surrounded by industrial activities related to oil and natural gas extraction (with the majority closer than 90 km), no substantial local sources exist in the vicinity of NSA and previous studies have shown only limited advection ($8 \pm 2\%$) of air masses passing through the Prudhoe Bay area to NSA (Kolesar et al., 2017). Despite substantial differences in aerosol properties, the two coastal sites lie only 250 km apart, resulting in very similar synoptic scale forcing, as can be seen from the high correlation between both sites for pressure, temperature, humidity, and wind (Fig. 2). For both sites, north-easterly to easterly winds prevailed during ACME-V (Holdridge and Kyrouac, 1993). Additionally, we grouped observations closer than 90 km to the two more continental sites Toolik and Atqasuk into a third data set (labeled TOI).

Cloud properties were observed using a combination of forward scattering, optical array, and bulk probes. The particle size distributions were measured using the forward scattering Cloud Droplet Probe (CDP) manufactured by Droplet Measurement Technologies (DMT), Inc.; the Fast Cloud Droplet Probe (FCDP) from Stratton Park Engineering Company (SPEC), Inc.; Two

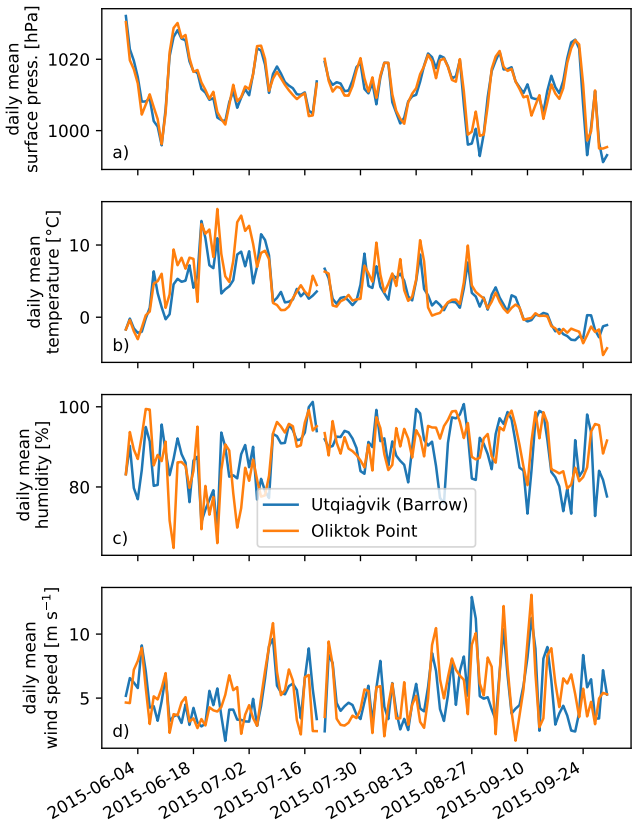

Figure 2. Comparison of daily mean values for a) surface pressure, b) 2 m temperature, c) 2 m humidity, and d) 10 m wind speed.

Dimensional Stereo optical array probes (OAPs) (2DS, Lawson et al., 2006); and the High Volume Precipitation Spectrometer (HVPS, Lawson et al., 1993) from SPEC, Inc. The raw OAP datasets were processed by the University of Illinois Optical Array Probe Processing Software (Wu and McFarquhar, 2016). In order to merge the cloud droplet size distributions, FCDP data were used for particles less than 50μm size, the 2DS was used for particles between 50 and 605 μm, and the HVPS was used for all particles exceeding 605 μm. In this study, particle diameter is used in general to describe the size of cloud and aerosol particles. Liquid clouds were required to have at least 10^7 m^{-3} droplets (Lance et al., 2011). In order to remove ice clouds from the data set, the Holroyd habit classification was applied to 2DS and HVPS observations with 1 s temporal resolution, which classifies particles mainly based on a fine detail ratio $F = pd/a$, where p is perimeter, d is diameter and a is area (Holroyd, 1987). The habit classification scheme differentiates between spherical particles, tiny particles which are too small to be classified and various forms of ice crystals. Spherical particles were assumed to be liquid. Tiny particles appear only at the lower end of the 2DS ($<$ 105 μm) and HVPS ($<$ 1125 μm) size range. They were classified as ice only if other size ranges were not dominated by spherical particles. Otherwise, tiny particles were assumed to be liquid. Data points with more than 100 m^{-3} particles larger than 400 μm (Lance et al., 2011) classified as ice were removed from the data set. This ensures that observations of spherical ice particles falsely classified as liquid, which likely occur together with larger, more

complex shaped ice particles, were removed from the data set as well. Liquid water content (LWC) was obtained by integrating the merged droplet size distribution (DSD), because direct observations of LWC from the King probe (King et al., 1978) are affected by a decreasing sampling efficiency for (drizzle) drops greater than 30 μm diameter. Clouds that were observed for less than ten continuous seconds were discarded, while gaps of up to 5 s were permitted once in cloud. Considering the typical true airspeed of the G-1 of 95 m/s, this corresponds to 950 m and 475 m when flying in a straight line, respectively. Additionally, only vertically sampled clouds (i.e. the aircraft was constantly ascending or descending) with a sampled vertical extent of at least 20 m were included in this evaluation to allow for comparison of in-cloud microphysical observations with below-cloud aerosol properties in sections 5 and 6. Therefore, very thin and/or small clouds might be discarded inadvertently. To make the detection of cloud boundaries more robust, the cloud probe data were smoothed using a 10s running average. Except for the detection of the cloud boundaries, effects of the smoothing are negligible for the presented analysis. For liquid clouds, aerosols of the size range 100 nm to 3 μm were observed with the Passive Cavity Aerosol Spectrometer (PCASP model 100X, DMT Inc.). We expect particles measured by the PCASP to be mostly dry, because it was operated with an anti-ice heater. Kassianov et al. (2015) showed for the very same aircraft that this assumption leads to good agreement between calculated (using, among others, PCASP observations) and measured scattering properties. Unfortunately, another aerosol sampler (Ultra-High Sensitivity Aerosol Sizer, UHSAS) which is able to detect aerosols below the PCASP detection threshold of 100 nm did not operate during the majority of the ACME-V flights. Two Condensation Particle Counters (CPC, TSI, Inc. models 3025 and 3010, respectively) were used to observe total number concentrations of condensation nuclei (CN) for the size ranges 3 nm - 3 μm and 10 nm - 3 μm, respectively. Unless otherwise stated, only the CPC 3025 featuring a size range of 3 nm - 3 μm was used in this evaluation. Black carbon (BC), which results from incomplete combustion of biomass and fossil fuels (Schwarz et al., 2008; Bond et al., 2013; Lack et al., 2014), was measured with the Single Particle Soot Photometer (SP2, from DMT Inc.), via incandescence. Thus, only refractory black carbon (rBC) is observed by the instrument. A counter for cloud condensation nuclei (CCN) was not deployed during ACME-V.

While Arctic Haze was not observed during ACME-V, transported emissions from forest fires can contribute significantly to summertime aerosol loading in the Arctic (Law and Stohl, 2007). Therefore, we manually inspected the vertical profiles of rBC and carbon monoxide (CO), which together constitute a good tracer for biomass burning (Warneke et al., 2009, 2010). Typically, these layers are found aloft (Roiger et al., 2015), allowing us to use vertical profiles to aid in their identification. The manual inspection was supported by aerosol dispersion simulations executed using version 4 of the Hybrid Single Particle Lagrangian Integrated Trajectory (HYSPLIT) model (Stein et al., 2015). These simulations were forced using 1° data from the NOAA/NCEP Global Data Assimilation System (GDAS) (Kalnay et al., 1996). Five locations were included as sources ((1) 62.096°N, 163.632°W, (2) 63.843°N, 159.046°W, (3) 65.294°N, 154.386°W, (4) 66.631°N, 149.023°W, and (5) 67.631°N, 144.087°W) and toggled on or off on a daily basis in correspondence to thermal anomaly observations from the Moderate Resolution Imaging Spectroradiometer (MODIS) on the Aqua and Terra satellites obtained using brightness temperature measurements in the 4 and 11 μm channels. (Giglio et al., 2003; Giglio, 2013). From each fire location, particle mass concentrations were simulated for 72 h at 100-m intervals from 0 to 5,000 m above ground level (m AGL). Both dry and wet deposition were considered for particles using the default HYSPLIT parametrizations (particle density 6 g cm^{-3}, shape factor 1.0). The particle

diameter of 0.2 μm used for the simulations is based on previous observations from fossil fuel and biomass burning sources (Brock et al., 2011; Eck et al., 1999; Rissler et al., 2006; Sakamoto et al., 2015). A dry deposition velocity of 1 x 10^{-4} m s^{-1} was assumed according to Warneck (1999) while 4 x 10^{4} L L^{-1} and 5 x 10^{-6} s^{-1} were used to account for in-cloud and below-cloud scavenging, respectively. Radioactive decay and pollutant resuspension were not considered. Note that the data impacted by forest fires were only removed for spirals above OLI, NSA, and TOI. For clear-air observations during level flight legs between sites, it is generally impossible to distinguish aerosols originating from forest fires as compared to other sources. Therefore, data potentially impacted by forest fires have only been removed from the cloud observations which have been associated with vertical profiles (Sec. 4f), but not from the aerosol observations presented in Sec. 3.

3 Aerosol properties

The spatial distributions of aerosol observations below 500 m MSL are presented for the CPC, the SP2, and the PCASP in Fig.3. The data presented are limited to observations obtained below 500 m in order to demonstrate the impact of local emissions and reduce the impact of forest fires. Furthermore, data flagged as sampled in cloud using the thresholds described in the previous section have been discarded in the analysis of aerosol properties due to concerns of contamination of the statistics by cloud droplets.

For the SP2, a clear local maximum of rBC concentration is visible east of OLI within the 90 km radius where most petroleum and gas extraction facilities are located (Fig. 1). A comparison of the distributions measured within a 90 km radius around the facilities reveals that the median of rBC concentration is the same for both regions (4 ng kg^{-1}). The tail of the distributions towards larger concentrations, however, is much greater at OLI (90th and 99.9th percentile 15 ng kg^{-1} and 42 ng kg^{-1}, respectively) than at NSA (17 ng kg^{-1} and 198 ng kg^{-1}, respectively). This enhancement is most likely connected to local emissions. CN measurements from the CPC show a similar pattern even though the increased values are distributed over a larger area. For both instruments, the distributions within the 90 km circle belonging to each site are skewed towards higher concentrations. Further, the difference between both CPC instruments, which depends on the concentration of CN between 3 and 10 nm diameter, is enhanced east of OLI (not shown). Freshly emitted soot has been shown to be larger than this ($>$ 20 nm), so this range is likely due to in situ nucleation of aerosol particles from gas phase precursors (i.e., formation of new particles as compared to secondary aerosol formation, where gases condense onto preexisting aerosol, Kulmala et al., 2012). Nucleated aerosols typically have sizes below 3 nm, but quickly grow via condensation and coagulation to sizes > 3 nm (Colbeck and Lazaridis, 2014). This source of nucleated aerosol particles from petroleum and gas extraction activities has been reported by Kolesar et al. (2017) for emissions transported from OLI to NSA. Unfortunately, we cannot analyze this aerosol nucleation process in more depth given limitations with the instrumentation operated during ACME-V. rBC concentrations appear to be similar to values found by Zamora et al. (2016) (1-16 ng/m3) and Roiger et al. (2015) (median 20-30 ng/kg) for summertime transported forest fire plumes in the Arctic. Other studies (Warneke et al., 2009; Schwarz et al., 2010) found up to one order of magnitude higher rBC concentrations in the Arctic which is more similar to the maximum values we observed around OLI. In

contrast to traces from forest fires, carbon monoxide (CO) concentrations were not found to be significantly enhanced in the OLI region (not shown).

The PCASP, which detects only particles larger than 100 nm, shows no spatial trends in the vicinity of the two sites. The comparison of the distributions around the facilities shows that the number of aerosols observed by the PCASP is on average actually slightly larger for NSA than for OLI. This is related to the fact that the median of the distribution is at 97 cm^{-3} at NSA and at 76 cm^{-3} at OLI. Similar to rBC, the tail of the distributions towards larger concentrations is greater at OLI (90th percentile 200 cm^{-3}) than at NSA (184 cm^{-3}). While it is challenging to clarify the precise cause of the increased mean concentration in detail, we speculate it might be related to transported emissions, including those from forest fires, that have not been properly removed from the data set. An alternative explanation could be the fact that collision-coalescence and precipitation rates are larger at NSA than at OLI (see next Sec. 4.) resulting in more aerosol processing by precipitation (e.g. Hoppel et al., 1990). Cloud-based processing leads to a reduction in aerosol concentration and an increase in aerosol size through conglomoration of cloud droplets (and corresponding aerosol particles) in the drizzle formation stage and subsequent evaporation. Such effects could increase the number of aerosols within the PCASP measurement size range.

To investigate why there is a clear enhancement in the CPC concentrations but not in the PCASP concentrations, both instruments sets are compared for all non-cloud observations below 500 m MSL during ACME-V. Fig. 4 shows CN concentration versus PCASP mean particle size and PCASP number concentrations for the two 90 km radii around OLI and NSA. It clearly illustrates that elevated CPC concentrations (> 600 cm^{-3}) found at NSA are typically connected with increased PCASP concentrations (> 100 cm^{-3}). While mean particle size generally increases with decreasing CN concentration, the variability of PCASP mean size is rather low for CN concentrations > 600 cm^{-3}, which is consistent with the idea that particles have already experienced growth. For OLI, on the other hand, variability in PCASP mean size is much larger. In addition, increased CPC CN concentrations do not necessarily correlate to increased PCASP particle concentrations at OLI. This means that for enhanced CN concentrations, which likely indicate a local source, PCASP particle concentrations can be small, but mean particle size is still significantly larger than 100 nm. The lower concentration and the higher size variability observed at OLI is consistent with the idea that particles in this region are younger. The value of 100 nm is important because it is assumed to be the size threshold between particles in Aitken mode and accumulation mode and typically only the latter can act as a CCN. (We do, however, note that smaller particles can act as CCN in very clean conditions (Leaitch et al., 2016).) In summary, aerosol particle sizes are more diverse at OLI and elevated CN concentrations are accompanied by enhanced PCASP mean particle sizes even though total PCASP particle concentrations are lower at OLI. Additional evidence for significant differences in aerosol concentrations between the sites is found in the fact that particle concentration of 600 cm^{-3} is exceeded in 62% of all cases at OLI, but only 35% at NSA.

4 Cloud properties

Here, cloud properties are compared for flights occuring near NSA and near OLI. In order to evaluate a sufficiently large sample, all observations obtained closer than 90 km to NSA, OLI and the two sites comprising TOI are assigned to the corresponding

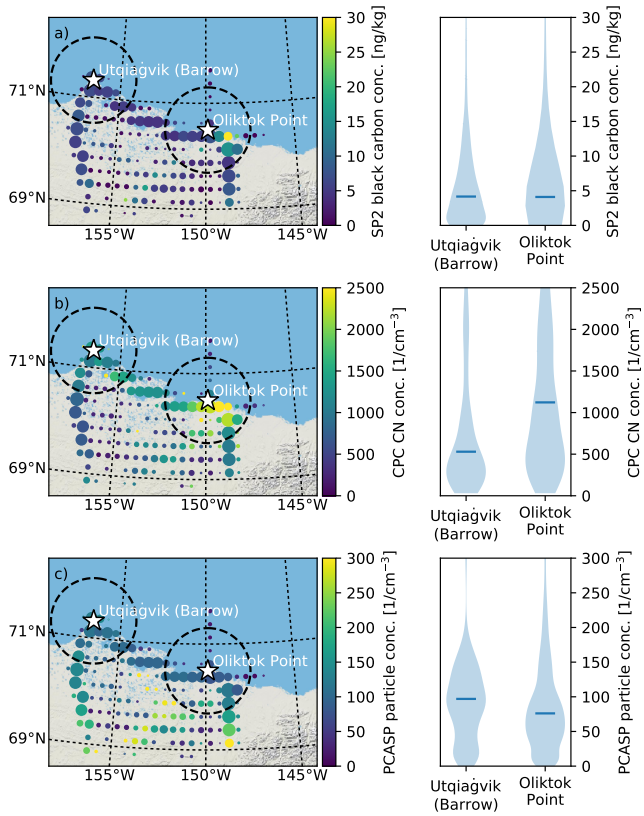

Figure 3. Left column: Spatial distribution of SP2 refractory black carbon concentration (a), CPC3025 CN concentrations (b), and PCASP aerosol concentration (c). Only non-cloudy observations below 400 m MSL have been considered. The size of the dots is proportional to the number of observations. The dashed circles correspond to a distance of 90 km. Right column: Here, the distribution of measurements within the 90 km circles are shown. The horizontal bar denotes the median value .

site (Fig, 1). As mentioned above, clouds impacted by forest fires have been removed. This limits the number of observations to 1608 1 s data points for OLI, 942 for NSA, and 579 for TOI.

When comparing 2D histograms of liquid effective radius and liquid water content for OLI and NSA (Fig. 5, a, b), a shift towards smaller r_{eff} can be clearly seen in the measurements obtained in close proximity to OLI. This supports our hypothesis that CCN concentrations are elevated in the OLI region, since the first aerosol-cloud indirect effect proposes that droplet size is reduced when more CCN are available (all else equal). While droplet r_{eff} observed at NSA cover the full range from droplet nucleation to drizzle (3 to 25 μm, mean 12.2$\pm$6.9 μm), r_{eff} values are typically smaller than 16 μm at OLI (mean 9.8$\pm$4.0 μm)

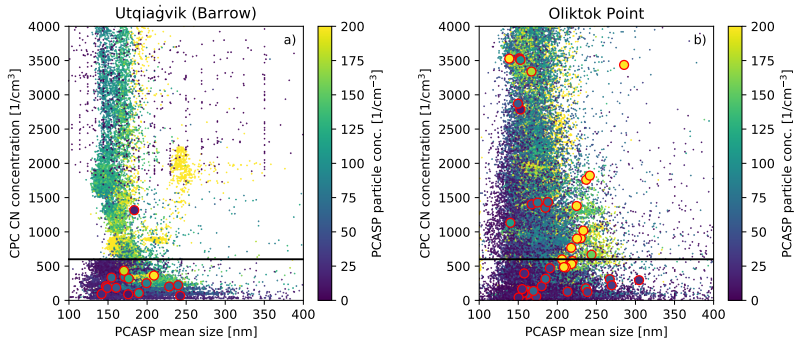

Figure 4. CPC3025 CN concentration versus PCASP mean particle size with PCASP particle concentration as color for (a) Utqiaġvik and (b) Oliktok Point. The black line corresponds to a CN concentration of 600 cm^{-3} The dots with red edges correspond to mean sub-cloud values corresponding to the clouds discussed in this study.

and observations of drizzle-sized droplets are rare. The value of 16 μm is of special interest because it was proposed by Gerber (1996) as a minimal effective radius required to initiate collision-coalescence. For comparison, data obtained in a 90 km radius around Toolik and Ivotuk (TOI) (Fig. 5, c). reveal that the distribution of observed r_{eff} at the coastal site in OLI is more similar to the inland sites comprising TOI (mean 7.2±3.1 μm) than to the second coastal site NSA.

The Albrecht effect proposes that more polluted clouds have longer cloud lifetime due to less efficient collision-coalescence (Albrecht, 1989). It is not possible to study the cloud life cycle using aircraft in-situ observations, but the potential for impact on cloud life cycle can be estimated by calculating the collection growth rate C (Long, 1974). C describes the mass of drops collected by a unit mass in a unit volume M per time interval t. It is the key process for converting cloud drops into precipitation and is estimated by integrating the mass collected by particles with diameter D_1 and mass m_1 over all size bins:

$$C = \frac{\mathrm{d}M}{\mathrm{d}t} = \int_{D_{\min}}^{D_{\max}} \frac{\mathrm{d}m_1}{\mathrm{d}t} N(D_1)\,\mathrm{d}D_1 \tag{1}$$

where $N(D_1)$ is the particle size distribution and $D_{\min}$ and $D_{\max}$ are the bounding drop diameters as determined by the cloud probes (0.75 μm and 8.7 mm). $\frac{\mathrm{d}m_1}{\mathrm{d}t}$ is obtained by integrating the collection kernel K for all smaller size bins (i.e. $D_1 > D_2$) described by the diameter of the collected drops D_2

$$\frac{\mathrm{d}m_1}{\mathrm{d}t} = \frac{\pi\rho_w}{6} \lim_{D_1 \to D'} \int_{D_{\min}}^{D'} K(D_1, D_2) N(D_2) D_2^3\,\mathrm{d}D_2 \tag{2}$$

where ρ_w is the density of liquid water. For simplicity, here we use a simple polynomial approximation of K

$$K(D_1, D_2) \approx \begin{cases} 5.78 \times 10^3 (v_1 + v_2) & 20 \le D_1 \le 100\mu m \\ 9.44 \times 10^9 (v_1^2 + v_2^2) & D_1 > 100\mu m \end{cases} \tag{3}$$

where v_i is the drop volume corresponding to D_i (Long, 1974; Pruppacher and Klett, 2010). Typical values range from 1×10^{-16} kg m^{-3}s for LWC = 0.001 g m^{-3} to 1×10^{-5} kg m^{-3}s for LWC = 1 g m^{-3}. Because we are interested how C is modified in the OLI region, we show the difference of C between both sites in Fig. 6 as a function of r_{eff} and LWC. It can be seen that C is decreased at OLI in comparison to NSA by up to one order of magnitude for constant LWC and r_{eff}. This is caused by reduced broadening of the drop size distribution towards large drops at OLI (not shown), consistent with cloud chamber experiments (Gunn and Phillips, 1957). Interestingly, differences in C are largest for r_{eff} smaller than 16 μm where absolute values of C are small according to Gerber (1996). However, small absolute increases in C for small r_{eff} are also crucial for triggering the positive feedback of drop growth due to collision-coalescence. When evaluating the potential impact of reduced C on cloud life cycle, one also has to consider that typical r_{eff} values are reduced at OLI in comparison to NSA for the same LWC (Fig. 5, a, b). Therefore, we estimate the mean growth rate $\bar{C}$ averaged over r_{eff} as a function of LWC (Fig. 6, a) red lines). Doing so reveals that, for constant LWC, $\bar{C}$ is reduced by 1 to 1.5 orders of magnitude at OLI. The offset is surprisingly constant for LWC larger than 0.01 g m^{-3}. Differences in C also translate to different rain rates R, which can be estimated by integrating the measured DSD and applying the fall velocity parametrization of Khvorostyanov and Curry (2002). Like C, R is reduced by up to one order of magnitude for constant LWC and r_{eff} (Fig. 6, b). Averaging over all r_{eff} enhances the effect and leads to differences of up to two orders of magnitude for R as a function of LWC.

Parameterizations of C and R are crucial in numerical models to transform cloud liquid water into rain droplets and to remove condensate from the atmosphere. Typically, numerical weather and climate models include either one (LWC, one-moment schemes) or two (LWC and drop concentration or r_{eff}, two-moment schemes) prognostic variables per hydrometeor species. Our comparison of C and R for both sites reveals, however, that these quantities vary by up to one order of magnitude for constant LWC and r_{eff} (which would be equivalent to a two-moment scheme). Considering only LWC (i.e. one-moment scheme) increases the differences to 1.5 to 2 orders of magnitude. As a consequence, additional moments or the full particle size distribution need to be considered in order to accurately estimate C and R in these models. Otherwise, a parametrization of C or R relying only on LWC (LWC and r_{eff}) might be biased up to 1.5 to 2 (1) orders of magnitude for one-moment (two-moment) schemes.

Even though the rate of mass removal from a cloud is an important process impacting cloud life cycle, it is important to note that modifications to C and R cannot be directly translated into modifications in cloud lifetime. This is because a reduction in R could result in a number of feedbacks such as cloud deepening (Stevens and Feingold, 2009) or reduced evaporation just below cloud base (Jiang and Feingold, 2006; Feingold and Siebert, 2009) that would act to counter the the extending effect of reduced precipitation rate on cloud lifetime.

5 Cloud-Aerosol interaction

So far, we have demonstrated that there are differences in aerosol properties and cloud properties between NSA and OLI. This is in general agreement with the findings of Hobbs and Rangno (1998) who found an increase in droplet number concentration

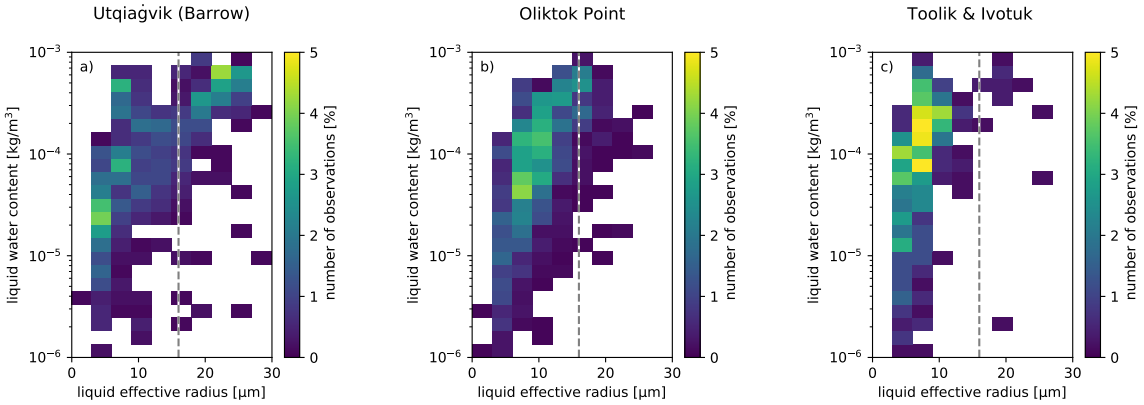

Figure 5. 2D-Histogram of number of observations as a function of effective radius r_{eff} and liquid water content LWC for Utqiaġvik/Barrow (a, 942 observations), Oliktok Point (b, 1608 observations) and Ivotuk/Toolik (c, 579 observations).

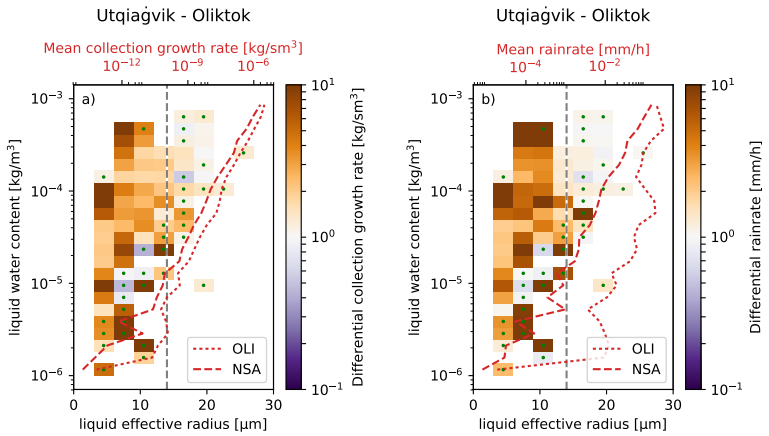

Figure 6. As Fig. 5, but with the difference OLI - NSA of the collection kernel growth rate C (a) and the rainrate R (b) as color. the rates averaged over r_{eff} are shown in red for OLI (dotted) and NSA (dashed). The green dots highlight data points with less than five observations.

when flying over Prudhoe Bay. In this section, we present evidence that these changes are indeed connected to local industrial activities centered around the Prudhoe Bay oil fields.

In order to evaluate the likelihood that Prudhoe Bay emissions impacted different portions of the ACME-V flights, we use the HYSPLIT dispersion model. Simulations were completed using one continuously emitting source located over the Prudhoe Bay oilfields (70.2556°N, 148.3384°W), using a configuration similar to that discussed above for evaluation of wildfire emissions. For OLI (NSA), 62% (16%) of all ACME-V cloud observations can be traced back to surface emissions originating from the Prudhoe Bay oilfields. The 16% determined for NSA is roughly twice that presented in Kolesar et al. (2017). However, they studied aerosol concentration at the surface instead of aloft and used a multi-year data set, which could introduce substantial variability from the 3-month period evaluated here. The HYSPLIT simulations (Fig. 7) show that the mass concentration

originating from local pollution sources is on average more than two order of magnitudes higher at OLI than at NSA. These simulations indicate that relative to NSA, the number of clouds impacted by local emission is increased at OLI and these clouds are impacted by a larger amount of aerosol particles by mass.

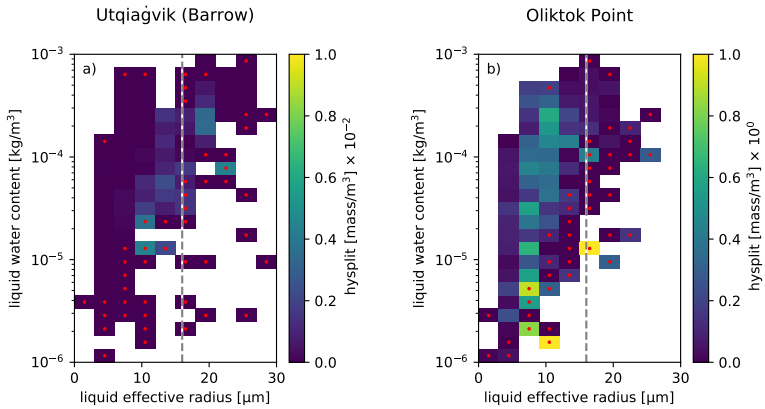

Figure 7. As Fig. 5, but with mass concentration of local emission according to the HYSPLIT model for OLI (a) and NSA (b). Note that the color scales for OLI and NSA differ by a factor of 100. The red dots indicate data points with less than five observations.

Fig. 8 relates in-cloud observations of LWC and r_{eff} to below-cloud observations of rBC similar to the approach of Jackson et al. (2012). This means that a single below-cloud aerosol value is assigned to every data point within the same cloud based on the assumption that aerosol properties are not changing on the scale of individual cloud profiles. The below-cloud values are averaged, whenever possible, over 30 seconds with a 3 second gap to the cloud base to avoid issues with time synchronisation across instruments or cloud particle contamination of aerosol probe measurements. Similar to Fig. 8, the below-cloud CPC CN concentration is shown in Fig. 9. These figures demonstrate clear relationships between cloud microphysics and rBC and CN (compare also Fig. 3). Around OLI, below-cloud rBC and CN values are increased, more than 10 ng kg^{-1} and 2000 m^{-3}, respectively. The coincidence of increased rBC concentrations with reduced r_{eff} might indicate that the observed rBC acted as a CCN. However this would require the rBC to be coated with more hygroscopic material (e.g. sulfate), because pure rBC does not serve as efficient CCN (Weingartner et al., 1997). While many of the CN detected by the CPC are likely too small to act as a CCN, these small particles can grow to accumulation mode quickly, potentially creating a particle population capable of acting as CCN (Jaenicke, 1980). It is interesting to note that despite the notion that elevated concentrations should result in smaller r_{eff}, these measurement indicate that local pollution are not connected to r_{eff} smaller than 9 μm. This is additionally supported by the reduced HSYPLIT mass concentrations (Fig. 7) for r_{eff} below 9 μm.

For the PCASP (Fig. 10), the aerosol concentration decreases more monotonically from small to large r_{eff} values. The fact that the response of r_{eff} to PCASP aerosol concentrations is very similar for both sites is likely because the PCASP covers the aerosol size range most relevant to droplet nucleation. It should be noted that the monotonic decrease in PCASP concentration with increasing droplet size is consistent with the first indirect effect. However, since no enhanced PCASP particle concentrations are found to be correlated to droplet sizes in the emissions-impacted 9 to 12 μm range (unlike for rBC

and CN), there is no indication that local emissions are directly altering liquid clouds to have smaller r_{eff} as a result of PCASP-sized particles. Even though similar PCASP concentrations lead to similar r_{eff} for both sites, differences still exist relating to the breadth and tail of the the distributions, as can be seen from differences in C and R (Fig. 6).

Fig. 4 also includes the below-cloud concentrations for CN and PCASP assigned to the clouds presented in this study (Note that—in contrast to the aerosols—clouds from all altitudes are shown). While for NSA, most clouds correspond to small CN concentrations, for OLI there are also clouds present corresponding to high CN values (i.e. potentially fresh emissions) most of which also feature high PCASP concentrations (> 200 cm^{-3}) with mean sizes > 200 nm. This indicates that even though CN measurements are dominated by Aitken mode particles, there are frequently sufficient CCN concentrations present to allow cloud formation. Because small particles can grow quickly into accumulation mode particles, these CCN might also originate from local sources.

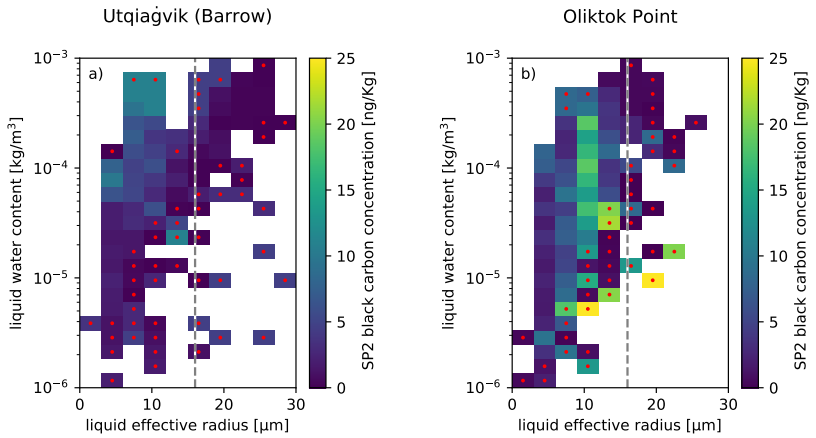

Figure 8. As Fig. 5, but with absolute values for SP2 refractory black carbon rBC concentration for (a) OLI and (b) NSA

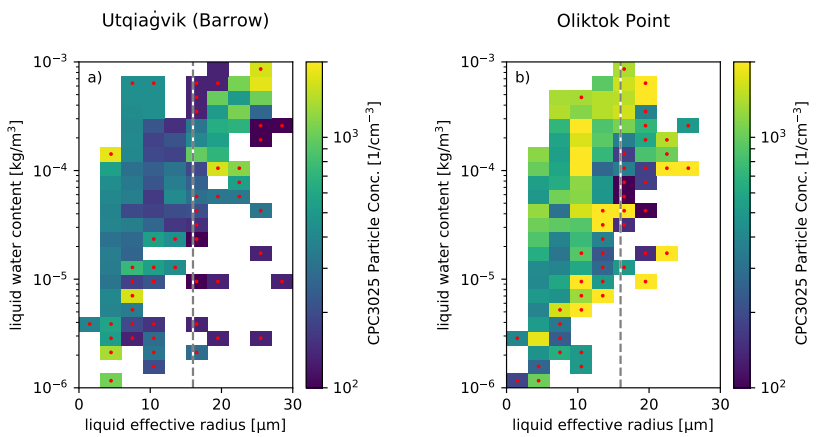

Figure 9. As Fig. 8, but with absolute values for CPC3025 condensation nuclei CN concentration.

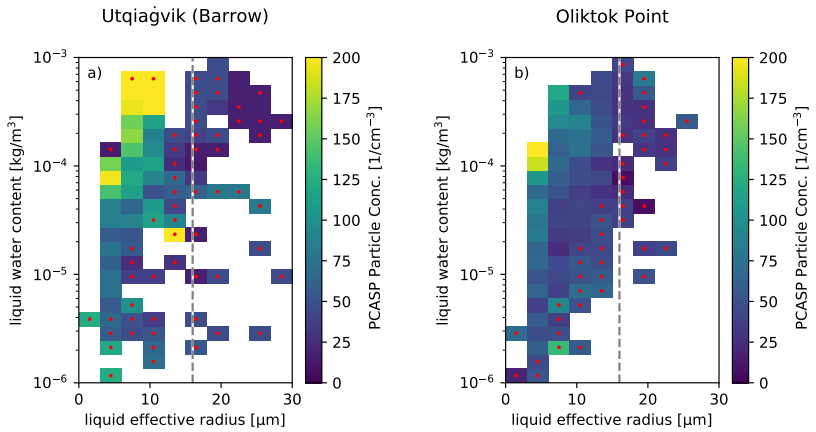

Figure 10. As Fig. 8, but with absolute values for PCASP particle concentration.

Finally, comparison of rBC size (Fig. 11) shows that black carbon particles are generally 50 to 300 nm smaller at OLI than at NSA. This is consistent with aging of rBC during atmospheric transport, and supports the idea that rBC measurements around OLI are associated with local emissions from Prudhoe Bay and not transported fire emissions. At NSA, this pattern of larger SP2 sizes is only interrupted for a small range of droplet r_{eff} between 9 and 12 μm, where both sites have similar mean sizes. This might be related to sampling issues, because this range coincides with very low rBC concentrations (Fig. 8) and low number of observations at NSA.

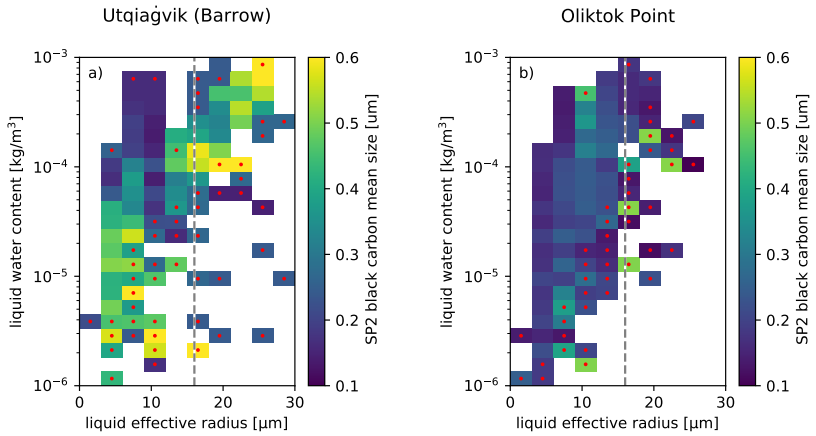

Figure 11. As Fig. 8, but with the mean size of refractory black carbon rBC measured below cloud.

6 Quantification of cloud aerosol interaction

Various attempts have been carried out to quantify aerosol cloud interaction (ACI) in Arctic regions (Coopman et al., 2016; Zamora et al., 2016) and its impact on radiation (Earle et al., 2011; Tietze et al., 2011). One common definition used for quantification purposes is:

$$ACI = \frac{1}{3}\frac{d\ln N_{\mathrm{tot}}}{d\ln N_{\mathrm{a}}} \tag{4}$$

with N_{tot} the number concentration of cloud droplets and N_a the number concentration of aerosols (Feingold et al., 2001; McComiskey et al., 2009). For observations, ACI is obtained using a linear regression of $\ln N_{tot}$ and $\ln N_a$. We prefer defining ACI using N_{tot} instead of r_{eff}, because the latter would require to classify the clouds by LWP, significantly reducing the size of the data set. Fig.12 shows N_{tot} and N_a for both sites. N_a is obtained form the PCASP because it covers the size range of active aerosols best. The ACI value for all clouds is 0.13 with R^2 = 0.23. Even though R^2 is small, the ACI value found here is similar to Zamora et al. (2016) who found ACI values of 0.15 for PCASP using a multi-campaign data set focused on biomass burning. McComiskey and Feingold (2012) found that the choice of platform and observational scales can have a significant impact on the estimation of ACI making comparisons between data sets challenging. Zamora et al. (2016), however, also used cloud-averaged in-situ aircraft observations and as a consequence we expect them to be comparable. When applying the linear regression to the data sets corresponding to the two sites separately, the obtained ACI values differ (Table 1), with OLI having a lower ACI value (0.1) than NSA (0.2). Given the small sample size (35 and 16 cases for OLI and NSA, respectively), it is not possible to answer the question of whether this is related to a difference in nucleation efficiency between aerosols at the two sites. The lower R^2 value for OLI (0.18) in comparison to NSA (0.40) could indicate that the assumption that PCASP particle concentrations represent a good approximation for CCN concentrations is partly violated at OLI. This could result from those particles being less aged and consequently less coated by sulfates and organics in comparison to those observed around NSA.

For comparison, we also evaluate ACI calculated using data points associated with forest fires. Based on the flight patterns executed, all of the cloud measurements associated with forest fire emissions were sampled in the vicinity of OLI. While fire emissions were also advected to the area surrounding NSA, cloud measurements from these time periods did not pass the quality control measures implemented (continuously ascending or descending profiles). Based on the measurements collected, aerosols associated with forest fires generally feature higher accumulation mode concentrations (and in consequence smaller r_{eff}), which is consistent with aging of these particles during transport, and in contrast to the freshly emitted particles generally found around OLI. When including cases associated with forest fire emissions, ACI is found to be 0.14 for both OLI and the complete data set, and is similar to results obtained when omitting forest fire influenced cases. Therefore, we conclude that a significant difference of ACI between local emissions and forest fires cannot be found given the limited data set.

7 Conclusions

The impact of local emissions from industrial activities in northern Alaska on liquid clouds has been investigated based on vertical profiles of aerosol and cloud properties during the ACME-V aircraft campaign, together with measurements from the

Table 1. ACI values for the subsets presented in Fig. 12

Data set	ACI	R^2	# clouds
all data	0.13	0.23	51
Oliktok Point	0.10	0.18	35
Utqiaġvik/Barrow	0.20	0.40	16
all data (with fires)	0.14	0.43	75
Oliktok Point (with fires)	0.14	0.44	59

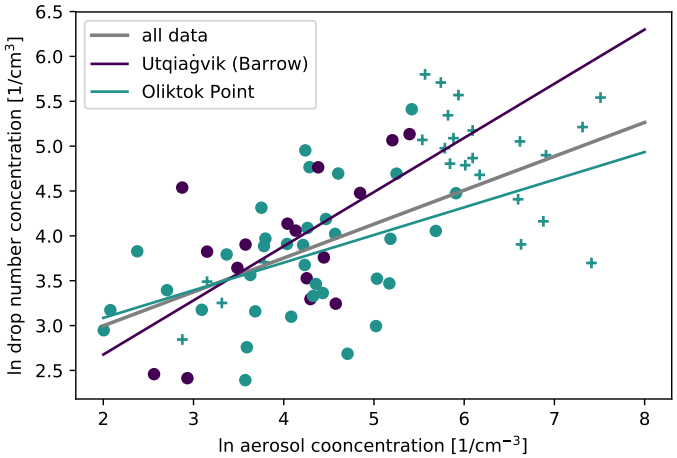

Figure 12. Aerosol indirect effect defined using cloud averaged cloud drop concentration N_{tot} and PCASP aerosol concentration N_a. The color is to differentiate between OLI (green) and NSA (purple). Clouds related to forest fires are marked with a '+'. The trend lines indicate the linear regressions to obtain ACI (excluding forest fires) for the complete data set (gray), NSA (purple) and OLI (green).

ARM sites in Northern Alaska: Oliktok Point (OLI) and Utqiaġvik (formerly known as Barrow or North Slope of Alaska, NSA). Our main findings can be summarized as follows:

1. Concentrations of condensation nuclei (CN) and refractory black carbon (rBC) are higher in the OLI area (Fig. 3). This is related to emissions associated with local oil and natural gas extraction activities. In contrast, concentrations of larger (diameter > 100 nm) particles are not elevated around OLI when compared to NSA.

2. In addition, we found (Fig. 5) that liquid clouds generally feature smaller r_{eff} at OLI (mean 9.8±4.0 μm) when compared with NSA (12.2±6.9 μm). Furthermore, collision-coalescence and precipitation rates are reduced by up to two orders of magnitude around OLI (Fig. 6). Only half of this reduction can be explained by the reduced r_{eff}. As a consequence, the breadth of the size distribution of liquid droplets has to be smaller at OLI.

3. Multiple lines of evidence connect these changes in cloud properties to the observed local emissions. First, HYSPLIT simulations show that 62% of all cloud observations around OLI can be traced back to local emission sources (Fig. 7). Second, reduced r_{eff} (between 9 and 12 μm) of OLI clouds correspond to increased CN and rBC concentrations (Figs. 8, 9). Third, the mean size of cloud-associated rBC particles is smaller at OLI which is consistent with freshly emitted, less aged particles (Fig. 11). Finally, while no enhanced concentrations of larger accumulation mode particles were observed for OLI (Fig. 3), clouds there were found to be frequently connected to enhanced CN and accumulation mode concentrations (Fig. 4).

4. Quantification of aerosol cloud interaction (ACI) is challenging due to the small data set. Having said this, the results from this study, based on evaluation of clouds impacted by both local emissions and forest fires, are consistent with previous studies of ACI in the Arctic environment (Fig. 12). While forest fire cases have typically higher aerosol concentrations and consequently droplet concentrations, their inclusion into the estimation of ACI does not substantially alter the found relationship.

Because only liquid clouds were observed during the majority of the flights, the impact of local pollution on mixed phase and pure ice clouds is not covered here. Moreover, the question whether the industrial activities at the North Slope of Alaska also lead to a change in local climate (e.g. due to cloud radiative forcing, precipitation impacts, or cloud life cycle), cannot be answered with in-situ aircraft measurements alone. These questions can likely better be answered using ground- and satellite-based remote sensing data from OLI and NSA by identifying differences between the sites in cloud cover, liquid water path, emissivity, effective droplet size, and precipitation occurrence. Nevertheless, based on this limited in-situ data set we can conclude that local emissions form industrial facilities in Alaska do influence local cloud properties while the overall spatial extent of these influences has yet to be evaluated. Given the observed cloud modifications, the effects of anthropogenic pollution on local climate should be considered when developing industrial infrastructure in an already fragile and warming Arctic environment.

8 Data availability

The surface observations from OLI and NSA as well as the ACME-V data set are available at the ARM archive www.arm.gov/data (Holdridge and Kyrouac, 1993; Biraud et al., 2016), the phase classification of the cloud probes is available form the corresponding author on request.

Acknowledgements. The authors would like to thank the teams of the ARM facilities (aerial, Olikotk Point, Utqiaġvik/Barrow) and the team responsible for processing and providing the data of the ACME-V campaign: among others S. Biraud, D. Chand, C. Flynn, J. Hubbe, C. Long, A. Matthews, M. Pekour, B. Schmid, A. Sedlacek, S. Springston, J. Tomlinson. Contributions from MM, GD and JC were supported by the US Department of Energy Atmospheric System Research (DOE ASR) program under award number DE-SC0013306. GD was additionally supported by NSF project ARC 1203902. GF was supported under DOE ASR grant No. DE-SC0016275; GM and WW were supported

under DOE ASR grant No. DE-SC0016476 (through UCAR subcontract Z17-90029). The authors gratefully acknowledge the NOAA Air Resources Laboratory (ARL) for the provision of the HYSPLIT transport and dispersion model used in this publication.

References

Albrecht, B. A.: Aerosols, Cloud Microphysics, and Fractional Cloudiness, Science, 245, 1227–1230, doi:10.1126/science.245.4923.1227, 1989.

Biraud, S., Mei, F., Flynn, C., Hubbe, J., Long, C., Matthews, A., Pekour, M., Sedlacek, A., Springston, S., Tomlinson, J., and Chand, D.: Campaign datasets for ARM Airborne Carbon Measurements (ARM-ACME-V), 2016.

Bond, T. C., Doherty, S. J., Fahey, D. W., Forster, P. M., Berntsen, T., DeAngelo, B. J., Flanner, M. G., Ghan, S., Kärcher, B., Koch, D., Kinne, S., Kondo, Y., Quinn, P. K., Sarofim, M. C., Schultz, M. G., Schulz, M., Venkataraman, C., Zhang, H., Zhang, S., Bellouin, N., Guttikunda, S. K., Hopke, P. K., Jacobson, M. Z., Kaiser, J. W., Klimont, Z., Lohmann, U., Schwarz, J. P., Shindell, D., Storelvmo, T., Warren, S. G., and Zender, C. S.: Bounding the role of black carbon in the climate system: A scientific assessment, J. Geophys. Res. Atmos., 118, 5380–5552, doi:10.1002/jgrd.50171, 2013.

Brock, C. A., Cozic, J., Bahreini, R., Froyd, K. D., Middlebrook, A. M., McComiskey, A., Brioude, J., Cooper, O. R., Stohl, A., Aikin, K. C., de Gouw, J. A., Fahey, D. W., Ferrare, R. A., Gao, R.-S., Gore, W., Holloway, J. S., Hübler, G., Jefferson, A., Lack, D. A., Lance, S., Moore, R. H., Murphy, D. M., Nenes, A., Novelli, P. C., Nowak, J. B., Ogren, J. A., Peischl, J., Pierce, R. B., Pilewskie, P., Quinn, P. K., Ryerson, T. B., Schmidt, K. S., Schwarz, J. P., Sodemann, H., Spackman, J. R., Stark, H., Thomson, D. S., Thornberry, T., Veres, P., Watts, L. A., Warneke, C., and Wollny, A. G.: Characteristics, sources, and transport of aerosols measured in spring 2008 during the aerosol, radiation, and cloud processes affecting Arctic Climate (ARCPAC) Project, Atmos. Chem. Phys., 11, 2423–2453, doi:10.5194/acp-11-2423-2011, 2011.

Colbeck, I. and Lazaridis, M.: Aerosol Science: Technology and Applications, John Wiley & Sons, 2014.

Colman, R.: A comparison of climate feedbacks in general circulation models, Climate Dynamics, 20, 865–873, doi:10.1007/s00382-003-0310-z, 2003.

Coopman, Q., Garrett, T. J., Riedi, J., Eckhardt, S., and Stohl, A.: Effects of long-range aerosol transport on the microphysical properties of low-level liquid clouds in the Arctic, Atmos. Chem. Phys., 16, 4661–4674, doi:10.5194/acp-16-4661-2016, 2016.

Earle, M. E., Liu, P. S. K., Strapp, J. W., Zelenyuk, A., Imre, D., McFarquhar, G. M., Shantz, N. C., and Leaitch, W. R.: Factors influencing the microphysics and radiative properties of liquid-dominated Arctic clouds: Insight from observations of aerosol and clouds during ISDAC, J. Geophys. Res., 116, D00T09, doi:10.1029/2011JD015887, 2011.

Eck, T. F., Holben, B. N., Reid, J. S., Dubovik, O., Smirnov, A., O'Neill, N. T., Slutsker, I., and Kinne, S.: Wavelength dependence of the optical depth of biomass burning, urban, and desert dust aerosols, J. Geophys. Res., 104, 31 333–31 349, doi:10.1029/1999JD900923, 1999.

Feingold, G. and Siebert, H.: Cloud-aerosol interactions from the micro to the cloud scale, in: Strüngmann Forum report, edited by Heintzenberg, J. and Charlson, R. J., The MIT press, Cambridge, MA, 2009.

Feingold, G., Remer, L. A., Ramaprasad, J., and Kaufman, Y. J.: Analysis of smoke impact on clouds in Brazilian biomass burning regions: An extension of Twomey's approach, J. Geophys. Res., 106, 22 907–22 922, doi:10.1029/2001JD000732, 2001.

Garrett, T. J. and Zhao, C.: Increased Arctic cloud longwave emissivity associated with pollution from mid-latitudes, Nature, 440, 787–789, doi:10.1038/nature04636, 2006.

Garrett, T. J., Zhao, C., Dong, X., Mace, G. G., and Hobbs, P. V.: Effects of varying aerosol regimes on low-level Arctic stratus, Geophys. Res. Lett., 31, L17 105, doi:10.1029/2004GL019928, 2004.

Gautier, D. L., Bird, K. J., Charpentier, R. R., Grantz, A., Houseknecht, D. W., Klett, T. R., Moore, T. E., Pitman, J. K., Schenk, C. J., Schuenemeyer, J. H., Sørensen, K., Tennyson, M. E., Valin, Z. C., and Wandrey, C. J.: Assessment of Undiscovered Oil and Gas in the Arctic, Science, 324, 1175–1179, doi:10.1126/science.1169467, 2009.

Gerber, H.: Microphysics of Marine Stratocumulus Clouds with Two Drizzle Modes, J. Atmos. Sci., 53, 1649–1662, doi:10.1175/1520-0469(1996)053<1649:MOMSCW>2.0.CO;2, 1996.

Giglio, L.: MODIS Collection 5 Active Fire Product User's Guide Version 2.5, 2013.

Giglio, L., Descloitres, J., Justice, C. O., and Kaufman, Y. J.: An Enhanced Contextual Fire Detection Algorithm for MODIS, Remote Sensing of Environment, 87, 273–282, doi:10.1016/S0034-4257(03)00184-6, 2003.

Gunn, R. and Phillips, B. B.: An experimental investigation of the effect of air pollution on the initiation of rain, J. Meteor., 14, 272–280, doi:10.1175/1520-0469(1957)014<0272:AEIOTE>2.0.CO;2, 1957.

Hobbs, P. V. and Rangno, A. L.: Microstructures of low and middle-level clouds over the Beaufort Sea, Q.J.R. Meteorol. Soc., 124, 2035–2071, doi:10.1002/qj.49712455012, 1998.

Holdridge, D. and Kyrouac, J.: ARM: ARM-standard Meteorological Instrumentation at Surface, 1993.

Holroyd, E. W.: Some Techniques and Uses of 2D-C Habit Classification Software for Snow Particles, J. Atmos. Oceanic Technol., 4, 498–511, doi:10.1175/1520-0426(1987)004<0498:STAUOC>2.0.CO;2, 1987.

Hoppel, W. A., Fitzgerald, J. W., Frick, G. M., Larson, R. E., and Mack, E. J.: Aerosol size distributions and optical properties found in the marine boundary layer over the Atlantic Ocean, J. Geophys. Res., 95, 3659–3686, doi:10.1029/JD095iD04p03659, 1990.

Intrieri, J. M., Fairall, C. W., Shupe, M. D., Persson, P. O. G., Andreas, E. L., Guest, P. S., and Moritz, R. E.: An annual cycle of Arctic surface cloud forcing at SHEBA, J. Geophys. Res., 107, 8039, doi:10.1029/2000JC000439, 2002.

Jackson, R. C., McFarquhar, G. M., Korolev, A. V., Earle, M. E., Liu, P. S. K., Lawson, R. P., Brooks, S., Wolde, M., Laskin, A., and Freer, M.: The dependence of ice microphysics on aerosol concentration in arctic mixed-phase stratus clouds during ISDAC and M-PACE, J. Geophys. Res., 117, D15 207, doi:10.1029/2012JD017668, 2012.

Jaenicke, R.: Atmospheric aerosols and global climate, Journal of Aerosol Science, 11, 577–588, doi:10.1016/0021-8502(80)90131-7, 1980.

Jeffries, M., Overland, J., and Perovich, D.: The Arctic shifts to a new normal, Physics Today, 66, 35–40, doi:10.1063/PT.3.2147, 2013.

Jiang, H. and Feingold, G.: Effect of aerosol on warm convective clouds: Aerosol-cloud-surface flux feedbacks in a new coupled large eddy model, J. Geophys. Res., 111, D01 202, doi:10.1029/2005JD006138, 2006.

Kalnay, E., Kanamitsu, M., Kistler, R., Collins, W., Deaven, D., Gandin, L., Iredell, M., Saha, S., White, G., Woollen, J., Zhu, Y., Chelliah, M., Ebisuzaki, W., Higgins, W., Janowiak, J., Mo, K. C., Ropelewski, C., Wang, J., Leetmaa, A., Reynolds, R., Jenne, R., and Joseph, D.: The NCEP/NCAR 40-year reanalysis project, Bulletin of the American Meteorological Society, 77, 437–471, 1996.

Kassianov, E., Berg, L. K., Pekour, M., Barnard, J., Chand, D., Flynn, C., Ovchinnikov, M., Sedlacek, A., Schmid, B., Shilling, J., Tomlinson, J., and Fast, J.: Airborne Aerosol in Situ Measurements during TCAP: A Closure Study of Total Scattering, Atmosphere, 6, 1069–1101, doi:10.3390/atmos6081069, 2015.

Khvorostyanov, V. I. and Curry, J. A.: Terminal Velocities of Droplets and Crystals: Power Laws with Continuous Parameters over the Size Spectrum, J. Atmos. Sci., 59, 1872–1884, doi:10.1175/1520-0469(2002)059<1872:TVODAC>2.0.CO;2, 2002.

King, W. D., Parkin, D. A., and Handsworth, R. J.: A Hot-Wire Liquid Water Device Having Fully Calculable Response Characteristics, Journal of Applied Meteorology, 17, 1809–1813, doi:10.1175/1520-0450(1978)017<1809:AHWLWD>2.0.CO;2, 1978.

Kolesar, K. R., Cellini, J., Peterson, P. K., Jefferson, A., Tuch, T., Birmili, W., Wiedensohler, A., and Pratt, K. A.: Effect of Prudhoe Bay emissions on atmospheric aerosol growth events observed in Utqiaġvik (Barrow), Alaska, Atmospheric Environment, 152, 146–155, doi:10.1016/j.atmosenv.2016.12.019, 2017.

Kulmala, M., Petäjä, T., Nieminen, T., Sipilä, M., Manninen, H. E., Lehtipalo, K., Dal Maso, M., Aalto, P. P., Junninen, H., Paasonen, P., Riipinen, I., Lehtinen, K. E. J., Laaksonen, A., and Kerminen, V.-M.: Measurement of the nucleation of atmospheric aerosol particles, Nat. Protocols, 7, 1651–1667, doi:10.1038/nprot.2012.091, 2012.

Lack, D. A., Moosmüller, H., McMeeking, G. R., Chakrabarty, R. K., and Baumgardner, D.: Characterizing elemental, equivalent black, and refractory black carbon aerosol particles: a review of techniques, their limitations and uncertainties, Anal Bioanal Chem, 406, 99–122, doi:10.1007/s00216-013-7402-3, 2014.

Lance, S., Shupe, M. D., Feingold, G., Brock, C. A., Cozic, J., Holloway, J. S., Moore, R. H., Nenes, A., Schwarz, J. P., Spackman, J. R., Froyd, K. D., Murphy, D. M., Brioude, J., Cooper, O. R., Stohl, A., and Burkhart, J. F.: Cloud condensation nuclei as a modulator of ice processes in Arctic mixed-phase clouds, Atmos. Chem. Phys., 11, 8003–8015, doi:10.5194/acp-11-8003-2011, 2011.

Law, K. S. and Stohl, A.: Arctic Air Pollution: Origins and Impacts, Science, 315, 1537–1540, doi:10.1126/science.1137695, 2007.

Lawson, R. P., Stewart, R. E., Strapp, J. W., and Isaac, G. A.: Aircraft observations of the origin and growth of very large snowflakes, Geophys. Res. Lett., 20, 53–56, doi:10.1029/92GL02917, 1993.

Lawson, R. P., O'Connor, D., Zmarzly, P., Weaver, K., Baker, B., Mo, Q., and Jonsson, H.: The 2D-S (Stereo) Probe: Design and Preliminary Tests of a New Airborne, High-Speed, High-Resolution Particle Imaging Probe, J. Atmos. Oceanic Technol., 23, 1462–1477, doi:10.1175/JTECH1927.1, 2006.

Leaitch, W. R., Korolev, A., Aliabadi, A. A., Burkart, J., Willis, M. D., Abbatt, J. P. D., Bozem, H., Hoor, P., Köllner, F., Schneider, J., Herber, A., Konrad, C., and Brauner, R.: Effects of 20–100 nm particles on liquid clouds in the clean summertime Arctic, Atmos. Chem. Phys., 16, 11 107–11 124, doi:10.5194/acp-16-11107-2016, 2016.

Long, A. B.: Solutions to the Droplet Collection Equation for Polynomial Kernels, J. Atmos. Sci., 31, 1040–1052, doi:10.1175/1520-0469(1974)031<1040:STTDCE>2.0.CO;2, 1974.

McComiskey, A. and Feingold, G.: The scale problem in quantifying aerosol indirect effects, Atmos. Chem. Phys., 12, 1031–1049, doi:10.5194/acp-12-1031-2012, 2012.

McComiskey, A., Feingold, G., Frisch, A. S., Turner, D. D., Miller, M. A., Chiu, J. C., Min, Q., and Ogren, J. A.: An assessment of aerosol-cloud interactions in marine stratus clouds based on surface remote sensing, J. Geophys. Res., 114, D09 203, doi:10.1029/2008JD011006, 2009.

McFarquhar, G., Ghan, S. J., Verlinde, J., Korolev, A., Strapp, J. W., Schmid, B., Tomlinson, J. M., Wolde, M., Brooks, S. D., Cziczo, D. J., Dubey, M. K., Fan, J., Flynn, C. J., Gultepe, I., Hubbe, J. M., Gilles, M. K., Laskin, A., Lawson, P., Leaitch, W. R., Liu, P. S., Liu, X., Lubin, D., Mazzoleni, C., Macdonald, A. M., Moffet, R. C., Morrison, H., Ovchinnikov, M., Shupe, M. D., Turner, D. D., Xie, S., Zelenyuk, A., Bae, K., Freer, M., and Glen, A.: Indirect and Semi-Direct Aerosol Campaign: The Impact of Arctic Aerosols on Clouds, Bull. Amer. Meteor. Soc., 92, doi:10.1175/2010BAMS2935.1, 2011.

Ødemark, K., Dalsøren, S. B., Samset, B. H., Berntsen, T. K., Fuglestvedt, J. S., and Myhre, G.: Short-lived climate forcers from current shipping and petroleum activities in the Arctic, Atmos. Chem. Phys., 12, 1979–1993, doi:10.5194/acp-12-1979-2012, 2012.

Peters, G. P., Nilssen, T. B., Lindholt, L., Eide, M. S., Glomsrød, S., Eide, L. I., and Fuglestvedt, J. S.: Future emissions from shipping and petroleum activities in the Arctic, Atmos. Chem. Phys., 11, 5305–5320, doi:10.5194/acp-11-5305-2011, 2011.

Platnick, S. and Twomey, S.: Remote sensing the susceptibility of cloud albedo to changes in drop concentration, Atmospheric Research, 34, 85–98, doi:10.1016/0169-8095(94)90082-5, 1994.

Pruppacher, H. R. and Klett, J. D.: Microphysics of Clouds and Precipitation, Springer, Dordrecht, 2 edn., 2010.

Quinn, P. K., Miller, T. L., Bates, T. S., Ogren, J. A., Andrews, E., and Shaw, G. E.: A 3-year record of simultaneously measured aerosol chemical and optical properties at Barrow, Alaska, J. Geophys. Res., 107, AAC 8–1, doi:10.1029/2001JD001248, 2002.

Quinn, P. K., Bates, T. S., Schulz, K., and Shaw, G. E.: Decadal trends in aerosol chemical composition at Barrow, Alaska: 1976–2008, Atmos. Chem. Phys., 9, 8883–8888, doi:10.5194/acp-9-8883-2009, 2009.

Rissler, J., Vestin, A., Swietlicki, E., Fisch, G., Zhou, J., Artaxo, P., and Andreae, M. O.: Size distribution and hygroscopic properties of aerosol particles from dry-season biomass burning in Amazonia, Atmos. Chem. Phys., 6, 471–491, doi:10.5194/acp-6-471-2006, 2006.

Roiger, A., Thomas, J.-L., Schlager, H., Law, K. S., Kim, J., Schäfler, A., Weinzierl, B., Dahlkötter, F., Krisch, I., Marelle, L., Minikin, A., Raut, J.-C., Reiter, A., Rose, M., Scheibe, M., Stock, P., Baumann, R., Bouarar, I., Clerbaux, C., George, M., Onishi, T., and Flemming, J.: Quantifying Emerging Local Anthropogenic Emissions in the Arctic Region: The ACCESS Aircraft Campaign Experiment, Bull. Amer. Meteor. Soc., 96, 441–460, doi:10.1175/BAMS-D-13-00169.1, 2015.

Sakamoto, K. M., Allan, J. D., Coe, H., Taylor, J. W., Duck, T. J., and Pierce, J. R.: Aged boreal biomass-burning aerosol size distributions from BORTAS 2011, Atmos. Chem. Phys., 15, 1633–1646, doi:10.5194/acp-15-1633-2015, 2015.

Schmid, B., Tomlinson, J. M., Hubbe, J. M., Comstock, J. M., Mei, F., Chand, D., Pekour, M. S., Kluzek, C. D., Andrews, E., Biraud, S. C., and McFarquhar, G. M.: The DOE ARM Aerial Facility, Bull. Amer. Meteor. Soc., 95, 723–742, doi:10.1175/BAMS-D-13-00040.1, 2014.

Schmid, B., Ellingson, R. G., and McFarquhar, G. M.: ARM Aircraft Measurements, Meteorological Monographs, 57, 10.1–10.13, doi:10.1175/AMSMONOGRAPHS-D-15-0042.1, 2016.

Schwarz, J. P., Gao, R. S., Spackman, J. R., Watts, L. A., Thomson, D. S., Fahey, D. W., Ryerson, T. B., Peischl, J., Holloway, J. S., Trainer, M., Frost, G. J., Baynard, T., Lack, D. A., de Gouw, J. A., Warneke, C., and Del Negro, L. A.: Measurement of the mixing state, mass, and optical size of individual black carbon particles in urban and biomass burning emissions, Geophys. Res. Lett., 35, L13 810, doi:10.1029/2008GL033968, 2008.

Schwarz, J. P., Spackman, J. R., Gao, R. S., Watts, L. A., Stier, P., Schulz, M., Davis, S. M., Wofsy, S. C., and Fahey, D. W.: Global-scale black carbon profiles observed in the remote atmosphere and compared to models, Geophys. Res. Lett., 37, L18 812, doi:10.1029/2010GL044372, 2010.

Shaw, G. E.: The Arctic Haze Phenomenon, Bull. Amer. Meteor. Soc., 76, 2403–2413, doi:10.1175/1520-0477(1995)076<2403:TAHP>2.0.CO;2, 1995.

Shupe, M. D. and Intrieri, J. M.: Cloud Radiative Forcing of the Arctic Surface: The Influence of Cloud Properties, Surface Albedo, and Solar Zenith Angle, J. Climate, 17, 616–628, doi:10.1175/1520-0442(2004)017<0616:CRFOTA>2.0.CO;2, 2004.

Stein, A. F., Draxler, R. R., Rolph, G. D., Stunder, B. J. B., Cohen, M. D., and Ngan, F.: NOAA's HYSPLIT Atmospheric Transport and Dispersion Modeling System, Bull. Amer. Meteor. Soc., 96, 2059–2077, doi:10.1175/BAMS-D-14-00110.1, 2015.

Stevens, B. and Feingold, G.: Untangling aerosol effects on clouds and precipitation in a buffered system, Nature, 461, 607–613, doi:10.1038/nature08281, 2009.

Stohl, A., Klimont, Z., Eckhardt, S., Kupiainen, K., Shevchenko, V. P., Kopeikin, V. M., and Novigatsky, A. N.: Black carbon in the Arctic: the underestimated role of gas flaring and residential combustion emissions, Atmos. Chem. Phys., 13, 8833–8855, doi:10.5194/acp-13-8833-2013, 2013.

Tietze, K., Riedi, J., Stohl, A., and Garrett, T. J.: Space-based evaluation of interactions between aerosols and low-level Arctic clouds during the Spring and Summer of 2008, Atmos. Chem. Phys., 11, 3359–3373, doi:10.5194/acp-11-3359-2011, 2011.

Twomey, S.: The Effects of Fluctuations in Liquid Water Content on the Evolution of Large Drops by Coalescence, J. Atmos. Sci., 33, 720–723, doi:10.1175/1520-0469(1976)033<0720:TEOFIL>2.0.CO;2, 1976.

Warneck, P.: Chemistry of the natural atmosphere, vol. 71, Academic press, 1999.

Warneke, C., Bahreini, R., Brioude, J., Brock, C. A., de Gouw, J. A., Fahey, D. W., Froyd, K. D., Holloway, J. S., Middlebrook, A., Miller, L., Montzka, S., Murphy, D. M., Peischl, J., Ryerson, T. B., Schwarz, J. P., Spackman, J. R., and Veres, P.: Biomass burning in Siberia and Kazakhstan as an important source for haze over the Alaskan Arctic in April 2008, Geophys. Res. Lett., 36, L02 813, doi:10.1029/2008GL036194, 2009.

Warneke, C., Froyd, K. D., Brioude, J., Bahreini, R., Brock, C. A., Cozic, J., de Gouw, J. A., Fahey, D. W., Ferrare, R., Holloway, J. S., Middlebrook, A. M., Miller, L., Montzka, S., Schwarz, J. P., Sodemann, H., Spackman, J. R., and Stohl, A.: An important contribution to springtime Arctic aerosol from biomass burning in Russia, Geophys. Res. Lett., 37, L01 801, doi:10.1029/2009GL041816, 2010.

Weingartner, E., Burtscher, H., and Baltensperger, U.: Hygroscopic properties of carbon and diesel soot particles, Atmospheric Environment, 31, 2311–2327, doi:10.1016/S1352-2310(97)00023-X, 1997.

Wu, W. and McFarquhar, G. M.: On the Impacts of Different Definitions of Maximum Dimension for Nonspherical Particles Recorded by 2D Imaging Probes, J. Atmos. Oceanic Technol., 33, 1057–1072, doi:10.1175/JTECH-D-15-0177.1, 2016.

Zamora, L. M., Kahn, R. A., Cubison, M. J., Diskin, G. S., Jimenez, J. L., Kondo, Y., McFarquhar, G. M., Nenes, A., Thornhill, K. L., Wisthaler, A., Zelenyuk, A., and Ziemba, L. D.: Aircraft-measured indirect cloud effects from biomass burning smoke in the Arctic and subarctic, Atmos. Chem. Phys., 16, 715–738, doi:10.5194/acp-16-715-2016, 2016.